Research Article | Vol. 13, No. 4 / 1 Apr 2022 / Biomedical Optics Express 2006
Biomedical Optics EXPRESS

Regression-based neural network for improving image reconstruction in diffuse optical tomography

GANESH M. BALASUBRAMANIAM* AND SHLOMI ARNON

Department of Electrical and Computer Engineering, Ben-Gurion University of the Negev, Be'er Sheva, 8441405, Israel
*ganesh@post.bgu.ac.il

Abstract: Diffuse optical tomography (DOT) is a non-invasive imaging technique utilizing multi-scattered light at visible and infrared wavelengths to detect anomalies in tissues. However, the DOT image reconstruction is based on solving the inverse problem, which requires massive calculations and time. In this article, for the first time, to the best of our knowledge, a simple, regression-based cascaded feed-forward deep learning neural network is derived to solve the inverse problem of DOT in compressed breast geometry. The predicted data is subsequently utilized to visualize the breast tissues and their anomalies. The dataset in this study is created using a Monte-Carlo algorithm, which simulates the light propagation in the compressed breast placed inside a parallel plate source-detector geometry (forward process). The simulated DL-DOT system's performance is evaluated using the Pearson correlation coefficient (R) and the Mean squared error (MSE) metrics. Although a comparatively smaller dataset (50 nos.) is used, our simulation results show that the developed feed-forward network algorithm to solve the inverse problem delivers an increment of ~30% over the analytical solution approach, in terms of R. Furthermore, the proposed network's MSE outperforms that of the analytical solution's MSE by a large margin revealing the robustness of the network and the adaptability of the system for potential applications in medical settings.

1. Introduction

Diffuse optical tomography (DOT) is a non-invasive imaging technology that uses visible and infrared light to identify tumors and other irregularities in human tissues [1,2]. DOT is non-invasive, has deep penetration, and causes no harm to patients during screening compared to other traditional imaging procedures such as X-ray mammography [3,4]. It is also far less expensive than traditional procedures such as MRI imaging [5,6]. DOT for breast cancer imaging has been explored in the past and found to have limited usefulness due to the scattering of visible and infrared light by human tissue and phenomena like optical blurring. However, there have been significant technological advances since then, such as increased computational efficiency leading to the development of novel deep learning algorithms [7,8] and a better overall understanding of the light propagation in tissues [9,10]. Due to this, DOT has found significant applications in tissue property estimation [7,8,11–13] and breast tissue imaging [4,14–17]. Therefore, we hope that it could be an effective, inexpensive, and safe screening method for a significant fraction of the population at risk in the near future.

Typically, imaging with tomography involves two steps: a forward problem and an inverse problem. The forward problem can commence when the bulk optical properties of the media are known [11,12]. In the forward problem [13–15], a non-ionizing light with a spectral range of 650 nm – 1100 nm is incident on the sample, and the tissue's optical properties [7,15] are probed using one of the three different tomographic models. These include continuous wave (CW), time-domain (TD), and frequency-domain (FD) techniques [6,16–19]. The collected data

#449448 https://doi.org/10.1364/BOE.449448
Journal © 2022 Received 23 Nov 2021; revised 8 Feb 2022; accepted 9 Feb 2022; published 11 Mar 2022

Biomedical Optics EXPRESS

using one or more of these modalities is then used to solve the inverse problem, which constitutes the second step in tomographic imaging. The inverse problem is an algorithm that is solved to accurately determine parameters such as the absorption and scattering coefficient of the medium, the size, and shape of the impurities, and to detect other anomalies in the media. However, the inverse problems used in DOT are solved using analytical methods, which are ill-posed, time and processing power consuming, and without good performance. Therefore, combining a deep learning algorithm with the inverse problem is urgent to improve performance.

Recent works have tried to mitigate these challenges by solving inverse problems using deep learning algorithms [11,20]. It is very clear from the latest literature that solving DOT using deep learning is faster, less complex, and more accurate [20–23]. This novel technology, which can broadly be classified as "Deep learning diffuse optical tomography," is becoming increasingly popular and has found applications in biomedical imaging [24–26], especially in the field of soft tissue imaging [11,23,27–29]. Jaejun Yoo et al. used a convolution neural network to invert the Lippman-Schwinger integral to solve DOT [20]. Here, a mean squared error (MSE) of 0.0049 ± 0.0012 and a Pearson coefficient (R) of 0.5657 are achieved. Hanene Ben Yedder et al. proposed a deep learning algorithm that can reconstruct images directly from DOT projection data with an MSE of 0.02 ± 0.03 and a structural similarity index (SSIM) of 0.46 ± 0.28 [21]. Furthermore, in a follow-up paper [23], an additional loss and transfer learning procedure were applied, and an enhancement was observed. In more recent work, a deep learning U-Net architecture has recently been developed in our lab to reconstruct detected anomalies in simulated compressed breast tissue using reflection tomography. Here, it is shown that deep learning algorithms enhance image reconstruction by ~55% [30]. In all the works mentioned above, the use of neural networks consistently outperforms the analytical solution approach. However, because of the intricate data models, DL requires a large quantity of data to function better than other algorithms, and it is somewhat expensive to train. DL models also need the usage of expensive GPUs and hundreds of workstations, raising the application's cost dramatically. Hence, a less complex but computationally efficient algorithm is required to solve inverse problems in DOT.

Over the past few years, regression-based feed-forward networks have been used for lung cancer classification [31], computed tomography [24,32], MRI imaging [25], and compressive sensing [33], with excellent results. A feed-forward network works by treating the forward process as a black box, reducing the system's complexity by using some form of initial mapping. The network then regresses to the error term by optimizing network parameters. Since regression-based algorithms are more dependent on the data points in each simulation, there is no need to create a large dataset, which saves time, and the simplicity of these systems makes them computationally efficient. However, such networks have not yet been implemented in diffuse optical tomography to the best of our knowledge. Therefore, this article designs a simple feed-forward network to solve the diffuse optical tomography problem in a compressed breast geometry to tackle this problem. The proposed neural network is more accurate and reduces the computational load on the system. The proposed approach, the neural network, and the network training methodology are described in section 2. Section 3 describes the image reconstruction process and discusses the results, and we end with the conclusions in section 4.

2. Solving the inverse problem of DOT using cascaded feed-forward networks

Solving the inverse problems in DOT requires complex solutions to complicated differential equations in the spatial, temporal, and spectral domains. Therefore, a cascaded feed-forward approach is proposed in this section to reduce the complexity of the DOT system and make the system faster. An introduction to the forward problem, the planned methodology to solve inverse problems in DOT, and the proposed feed-forward neural network architecture are described in this section.

Biomedical Optics EXPRESS

2.1. Forward and inverse problems in DOT: Simulating light propagation in tissues

The imaging and detection modality in DOT is based on the behavior of diffuse and multi-scattered photons when they travel through turbid media. The behavior of such photons is defined by the radiative transport equation given by [9,10,34]:

$$\frac{dJ(r,s)}{ds} = -(\mu_a + \mu_s)J(r,s) + \frac{\mu_s}{4\pi}\int_0^{4\pi} p(s,s')J(r,s')d\omega \tag{1}$$

where $J(r,s)$ is the radiance in $W\ cm^{-2}\ sr^{-1}$, $p(s,s')$ is the probability density function of a photon to be scattered from the direction s' to s, ds is infinitesimal path length and $d\omega'$ is the elementary solid angle about the direction s'. μ_a and μ_s are the absorption and scattering coefficient, respectively. However, Eq. (1) is difficult to solve analytically, and it is complicated further by the inability to separate the coherent and incoherent terms in the equation. Therefore, photon behavior in turbid media can be analyzed using the diffuse approximation, given by:

$$\frac{\partial\phi(r,t)}{c\partial t} + \mu_a\phi(r,t) - \nabla.[D\nabla\phi(r,t)] = S(r,t) \tag{2}$$

where D is the diffusion term defined as $D = 1/3(\mu_s' + \mu_a)$ and $S(r,t)$ is the source term assumed to be isotropic. In the diffuse approximation, the assumption is that the reduced scattering coefficient is much greater than the absorption coefficient, the source-detector location is large enough, and the thickness of the sample is very large ($\gg$ 10 times the mean free path.). The radiance is expressed as a weighted sum of the photon fluence rate (ϕ), which is the integral of the radiance over the entire solid angle, and the current density, $\overrightarrow{J}(\mathbf{r},t)$ defined as the net energy flow per unit area per unit time (t). Using Eq. (2) in the spatial, temporal, and spectral domains, a tomographic forward problem can be simulated using the finite element or Monte-Carlo methods [13–15,35].

The medium's optical parameters and spatial distribution of the optical properties are reconstructed from the simulated signals obtained from the forward problem. Reconstruction problems in DOT are part of a larger category of problems known as inverse problems [36], which have the following basic form:

$$Find\ \mathrm{x} \in X\ from\ data\ y = A(x) + \delta,\ y \in Y \tag{3}$$

where X is the optical parameters space, Y is the measurements space, A is the propagation model of photons convolved with the optical component response, and δ is the noise mechanism in the system. In DOT, Eq. (3) refers to the mapping between the optical properties of the media to the amplitude, phase, or time signals registered by the detectors.

Traditionally, inverse problems have been solved using iterative analytical methods [14,15,36,37]. However, large-scale application of high-quality DOT image reconstruction is yet to be accomplished since the technique requires a lot of processing power and spatio-temporal data, both of which are currently unavailable. Furthermore, the dearth of ballistic photons combined with the loss of imaging information due to repeated scattering occurrences creates a non-linear, ill-posed inverse problem, necessitating appropriate solutions to complete this difficult task. As a result, we propose a hybrid technique for tackling DOT inverse problems using a simple deep learning algorithm in the following sub-section.

2.2. Proposed methodology to solve inverse problems in DOT

In this study, we propose a simple deep learning neural network to solve inverse problems in DOT for the given dataset. The dataset is generated using a forward problem where the forward problem using the given bulk optical properties are simulated using the ValoMC software [13]

Biomedical Optics EXPRESS

(Monte-Carlo method). The simulated compressed breast tissues are modeled using the optical properties [12,38], and a test object of varying sizes is placed at random locations within the compressed breast. A parallel plate geometry is used in this study. The schematic of the proposed process is shown in Fig. 1.

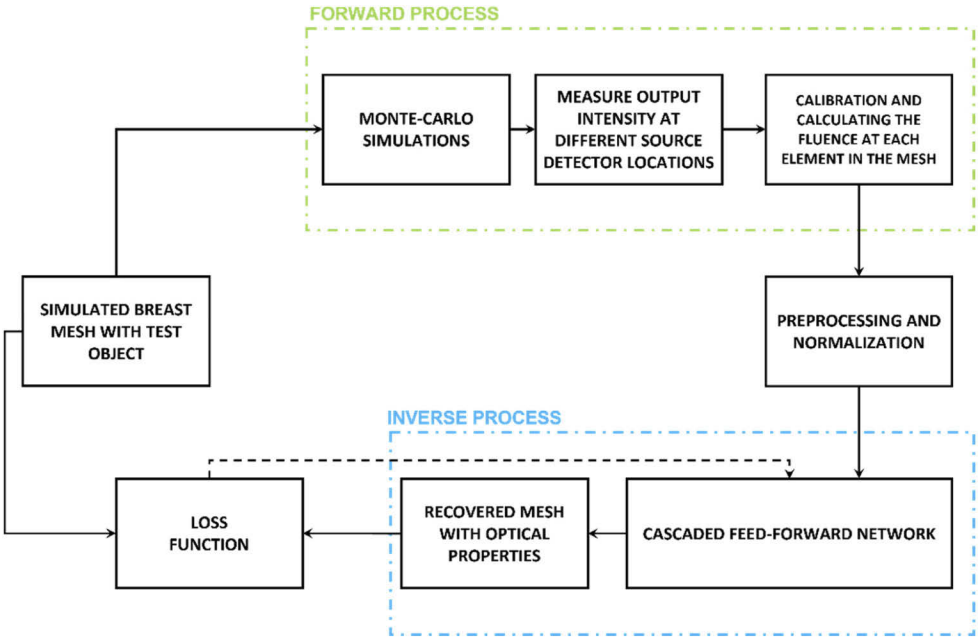

Fig. 1. Schematic of the proposed deep learning diffuse optical tomography method.

The proposed operation proceeds as follows:

1. *Mesh creation:* ValoMC [13] software is used to create the compressed breast geometry [39,40] and simulate light propagation in the tissue. The compressed breast tissue has the dimensions of 120 mm × 40 mm × 40 mm (height × width × thickness), and the compressed breast is modeled as an oblate spheroid of equatorial radius 60 mm and polar radius 40 mm, compressed between the source-detector glass plates. The homogeneous breast tissue and the test object (breast-tumor sphere) are given optical properties according to reference [12,41] and are modeled as spheres of radii 3 mm – 6 mm. Up to six test objects of varying radii but the same absorption and scattering coefficient are placed inside the breast tissue. The optical absorption coefficient, the reduced scattering coefficient, and the scattering anisotropy of the materials used in this manuscript are shown in Table 1.

2. *Forward process and data creation:* The light is propagated through the tissue containing anomalies using a Monte-Carlo algorithm [13], and the output light is collected according to the source-detector configuration shown in Fig. 2. The forward problem is implemented in the same way as Ref. [42], with some modifications due to the mesh-based geometry and path weighting differences. The Mersenne-Twister algorithm [43] is used to create random numbers. The geometry used for this study is akin to the slab geometry [40]. This type of geometry is chosen as it is one of the most common tomographic arrangements used in medical imaging of compressed breast tissue. This arrangement allows us to thoroughly illuminate the compressed breast tissue from both sides and collect the transmitted light. Here, photons are emitted from one of the sources, and simulated data is collected at the

Biomedical Optics EXPRESS

detector locations on the opposite plane. The simulations are conducted using 20 million photons for each simulation which are input as CW light. 50 simulated breast data are used in this study.

3. *Pre-processing:* This process helps us mitigate one of the significant problems in image reconstruction, which is the reconstruction algorithms' inability to determine the interfaces between various structures and the source-detector locations. Pre-processing the data before the network training also allows us to use more significant amounts of data while simultaneously reducing the load on the algorithm [44]. Moreover, calibrating and normalizing the fluence values at the boundaries allows us to better approximate the element fluence values and, hence, allows us to obtain better data. This, in turn, affects the training algorithm.

4. *Inverse process and anomaly detection by estimating the optical properties of the simulated media:* The calibrated output data is then fed to the cascaded feed-forward network. The proposed deep learning algorithm works by having the calculated fluence of each element in the mesh and determining the optical properties of anomalies present in the compressed breast. An analytical solution [13,21] is also employed to check for enhancement.

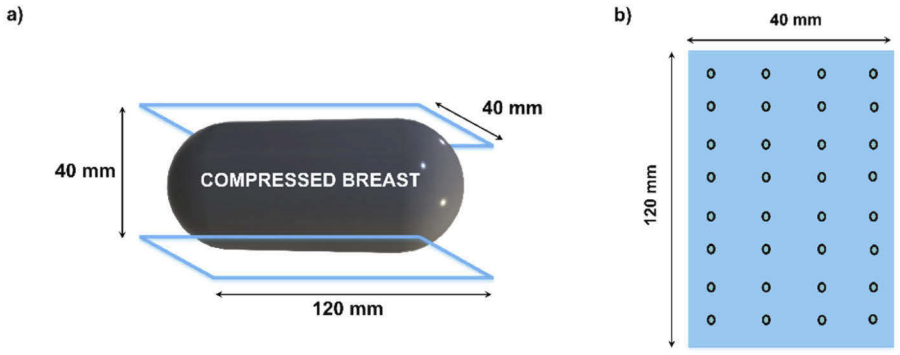

Fig. 2. a) The compressed breast geometry containing the spherical anomalies and b) Source-detector configuration used for tomographic reconstruction in this study.

Table 1. Optical properties of the materials used in the manuscript [41].

S. No.	Tissue	Wavelength	Absorption coefficient (μ_a)	Reduced scattering coefficient (μ_s')	Scattering anisotropy (g)
1.	Breast	670 nm	$0.011 \pm 0.006\ mm^{-1}$	$1.22 \pm 0.039\ mm^{-1}$	0.90
2.	Tumor	670 nm	$0.0036 \pm 0.008\ mm^{-1}$	$0.84 \pm 0.04\ mm^{-1}$	0.97

The proposed neural network is described in the next section

2.3. Cascaded feed-forward neural networks to solve inverse problems in DOT

Regression-based feed-forward networks work by determining the correlation between a dependent variable (element fluence, boundary fluence) and one or more independent variables (absorption and scattering coefficient). Unlike conventional regression models that do not fit the data perfectly, feed-forward neural networks are adaptable and can dynamically pick the best type of regression. Moreover, skip connections and hidden layers can be added to strengthen the regression model. The workflow of a regression-based cascaded feed-forward network is shown in Fig. 3.

Biomedical Optics EXPRESS

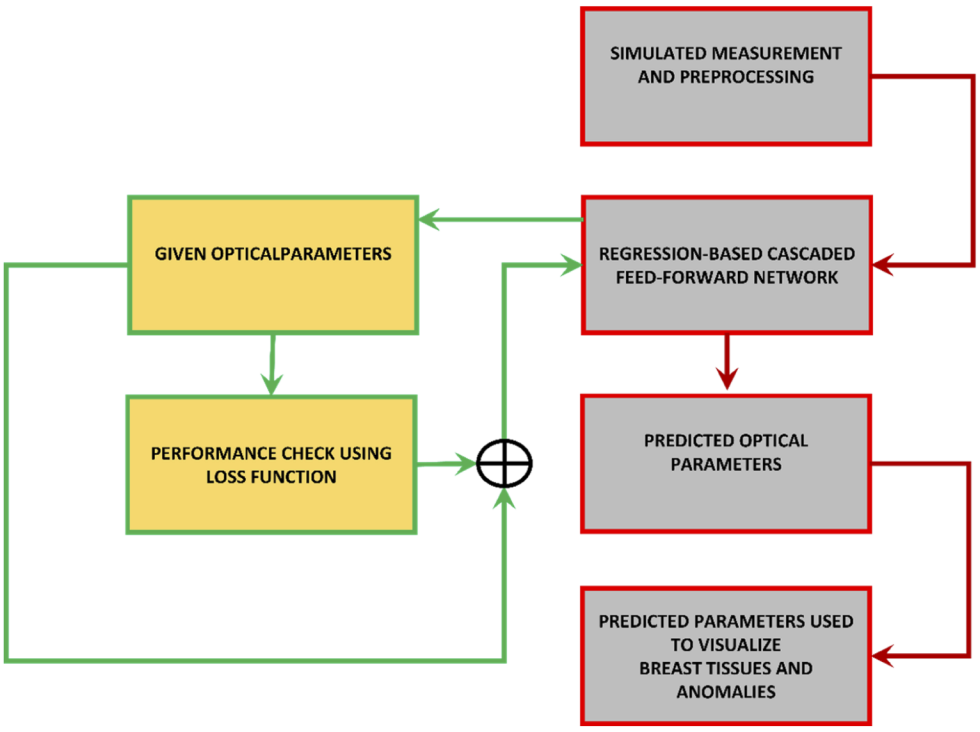

Fig. 3. Workflow of the proposed neural network. A rough approximation of the optical properties is achieved utilizing the simulated measurements. Then, It is residually connected to the network, which refines it and allows for a more accurate prediction and reconstruction.

In the cascaded feed-forward neural network architecture shown in Fig. 4 (a), a network with seven hidden layers is considered with a single output-input vector. The normalized dataset, obtained by calculating the fluence of every element in the mesh from the boundary output values, enters the first hidden layer with three neurons, where the algorithm adds weights and biases to the input and initiates the regression problem. Additional weights and biases are added in the further hidden layers with four, six, two, two, six, and three neurons, respectively (Fig. 4 (a)). Since each simulated breast tissue contains information from many voxels, additional skip connections are provided to every layer to form a fully-connect neural network for better feature extraction and add additional weights in the hidden layers. The structure of the neuron is represented in Fig. 4 b. The Levenberg-Marquardt (LM) function is used to train the feed-forward network, determine the weights and biases, and estimate the network parameters with a learning rate of 0.0001 [45]. The LM bridges the gap between the Gauss-Newton (GN) function and the gradient descent approach. Because the LM is more durable than the GN, it can often find a solution even when it starts very far from the final minimum. Also, when compared to first-order backpropagation approaches, the LM function frequently converges quicker.

The network is trained for 60 epochs, and the results of the proposed network and the training mechanism are described further in the next section. The proposed algorithm reduces the computational burden by mapping the input to physically possible solutions in the same space as the desired solution. Furthermore, the network output can be residually connected to the estimate instead of directly reconstructing based on the estimated inverse, which significantly enhances the regression process.

Biomedical Optics EXPRESS

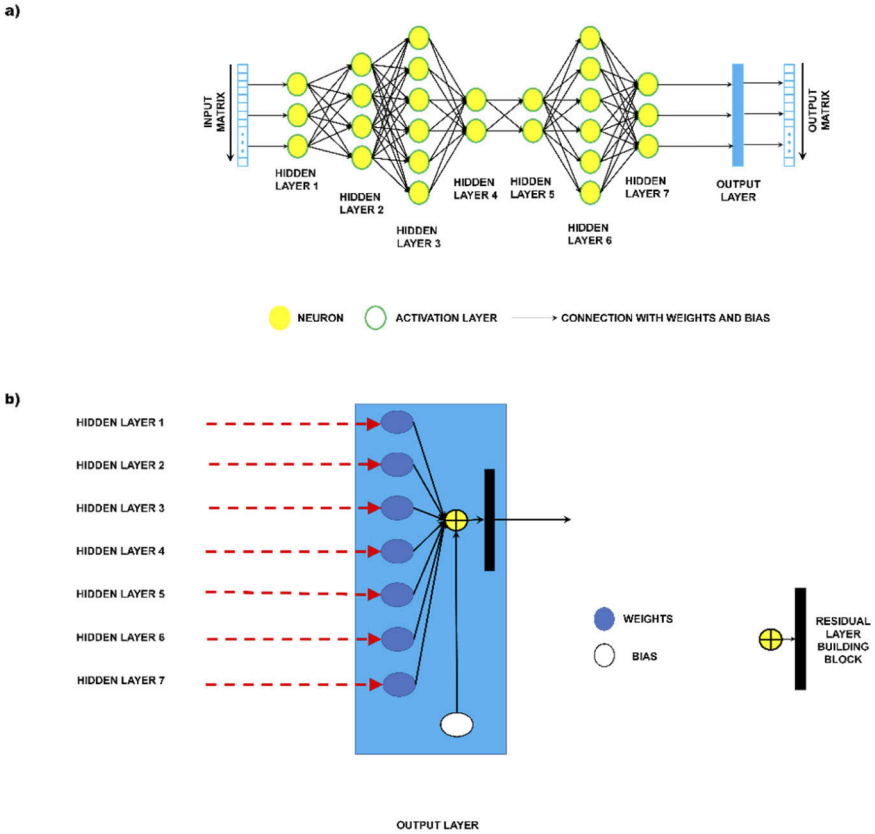

Fig. 4. a) Cascaded feed-forward network used to solve inverse problems in this study. b) Skip connections are also provided from one hidden layer to every other hidden layer and the output layer. The output layer is shown here, which is also the general structure of a neuron in the network.

3. Results and discussions

The neural network is built and trained on a computer with an i9 series 9900k processor with two NVIDIA GeForce RTX 2080Ti graphics processors. The network is trained for 60 epochs using the simulated compressed breast tissues with test objects. The simulated data from light propagation in the compressed tissues is taken for 50 breasts with up to 6 test objects of varying sizes as described in section 2.2 are placed in each breast. A total of 50 breast simulations were conducted. Forty-five of the simulated data are used for training (38 for training and 7 for validation), and the remaining five breast datasets are used for testing. The mean squared error (MSE) loss function is employed, and the Pearson correlation coefficient (R) is used to check the correlation between the neural network's predicted values and the ground truth. The model inputs are the approximate elemental fluence of all elements that are roughly calculated from the boundary fluence values. The model output is the predicted absorption coefficient values. Moreover, a 2% Gaussian noise was added to the simulated forward problem to mimic the noise and aberrations that might arise due to experimental hardware. The absorption coefficient and the fluence values are normalized using the min-max method to fix all the values between 0 and 1. Figure 5 shows the correlation of the analytical solution and the proposed cascaded feed-forward network to the ground truth values.

Biomedical Optics EXPRESS

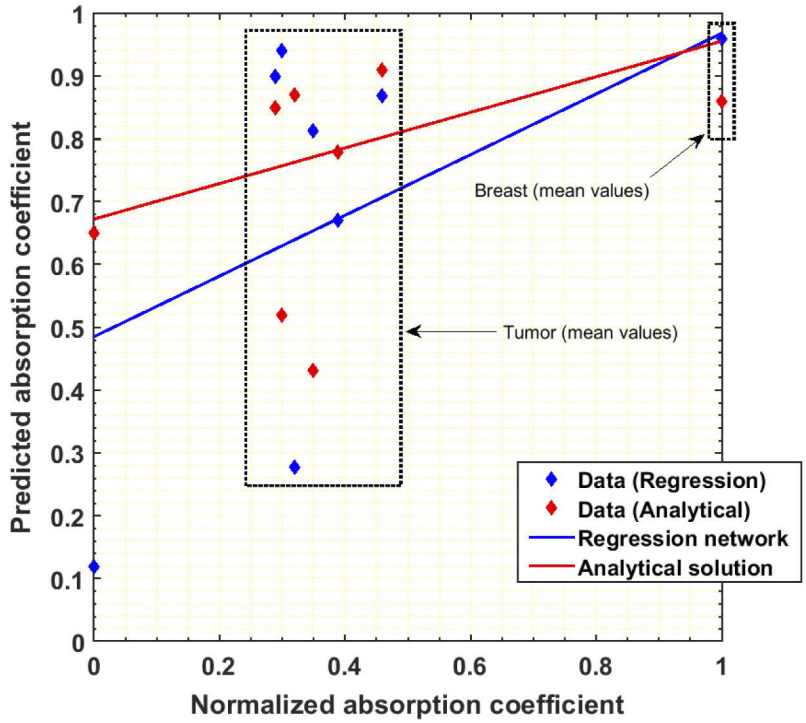

Fig. 5. Correlation graph for predicting the absorption coefficient of the background tissue and the test objects. The values on the x-axis show the normalized absorption coefficient of the simulated breast tissues with anomalies, and the y-axis shows the predicted absorption coefficient by the analytical solution and the regression neural network. The data points represent the mean predicted values by the analytical solution (red) and the regression neural network (blue).

The regression network provides a correlation of 0.692 ± 0.023 compared to 0.534 ± 0.037 when the analytical solution is used to solve the inverse problem. The better performance of the neural network method can be attributed to factors like the computational limitations of the analytical solution, which is heavily dependent on the location of the test objects and fluence mismatches created at the boundaries of the compressed breast-glass plate interface. These effects are minimized when the neural network approach is used. However, it has to be noted that using this method, one must be careful with the elemental mesh size and the size of the test objects. Too many data points may cause overfitting, and very few data points (large voxel size) may cause underfitting. Also, if the test objects are too small, it may lead to inaccuracies in determining the absorption coefficient. This is because the regression algorithm requires a certain amount of fluence distribution data for each absorption coefficient value to regress to the ground truth values.

Also, a performance of 0.0265 ± 0.0042 is observed in terms of the MSE when the neural network method is used. The training graphs for the system's performance are shown in Fig. 6. Each training iteration takes around 45 seconds to complete in terms of the computation time. Moreover, due to the bulk nature of the simulated breast tissues and the vast number of data points, the training performance converges around the 15 epoch mark. Therefore, ideally, each training phase takes about 11 minutes. However, unlike the analytical solution approach, the regression network can be trained in advance before validating new breast simulations, significantly reducing the time to detect anomalies in compressed breast tissues.

Biomedical Optics EXPRESS

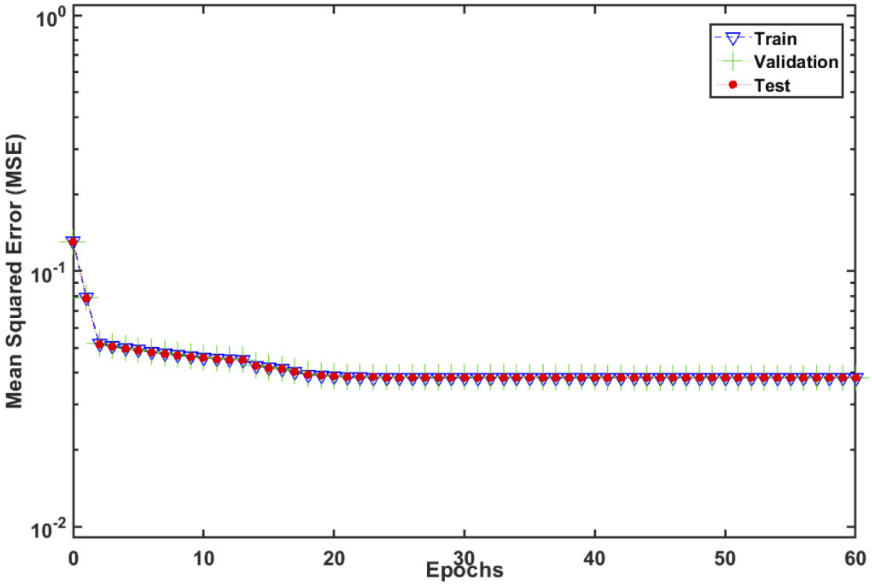

Fig. 6. Training graphs for the performance of the proposed neural network to solve the inverse problem in compressed breast tissues.

Following the training process, 5 different compressed breast tissues were used for validation, and the predicted data obtained using the analytical solution and the proposed neural network is fed to the ValoMC [13] software to visualize the reconstructed image. Figure 7 (a) shows the ground truths. The image reconstructions using data from the analytical solution and the proposed neural network are shown in Fig. 7 (b) and Fig. 7 (c), respectively. From Fig. 7, it can be seen that the analytical solution approach used to solve the inverse problem and reconstruct objects suffers from loss of resolution and contains significant errors. The sizes of the test objects are also not reconstructed accurately, and substantial blurring is observed at the boundaries of the test objects. Due to these factors and the ill-posedness of the analytical solution, this approach delivers a high and unsatisfactory MSE of 0.0612 ± 0.039. In stark contrast to the analytical method approach, the proposed neural network algorithm delivers an excellent MSE value of 0.0265 ± 0.0042 compared to the analytical solution approach. The image reconstruction is much smoother when the proposed cascaded feed-forward neural network data is used, clearly evident in Fig. 7 (c). The reconstructed breast boundaries are well defined, and the test objects of different sizes are accurately reconstructed in terms of location and size. Upon closer inspection, it is also clearly noticeable that the predicted absorption coefficient values are closer to the given absorption coefficient values (ground truths) when the proposed regression network is used, which shows the well-posedness of the deep learning algorithm to solve inverse problems for DOT and provide accurate data for image reconstruction.

On the other hand, the neural network approach has some limitations and difficulties. Aside from being very dependent on the dataset and network settings, the fundamental challenge with this type of research is that training a deep learning network using real-time experimental data is challenging due to the near impossibility of collecting such a vast quantity of experimental data. As a result, most deep learning techniques for DOT are trained on simulated datasets, resulting in precision and accuracy trade-offs in real-world studies. However, as can be seen from the article published by Jaejun Yoo et al. [20], it is possible to train the deep learning neural network using simulated datasets and still get excellent and accurate results when real tissues or phantoms are used. Therefore, simple, regression-based, end-to-end deep learning algorithms may be

Biomedical Optics EXPRESS

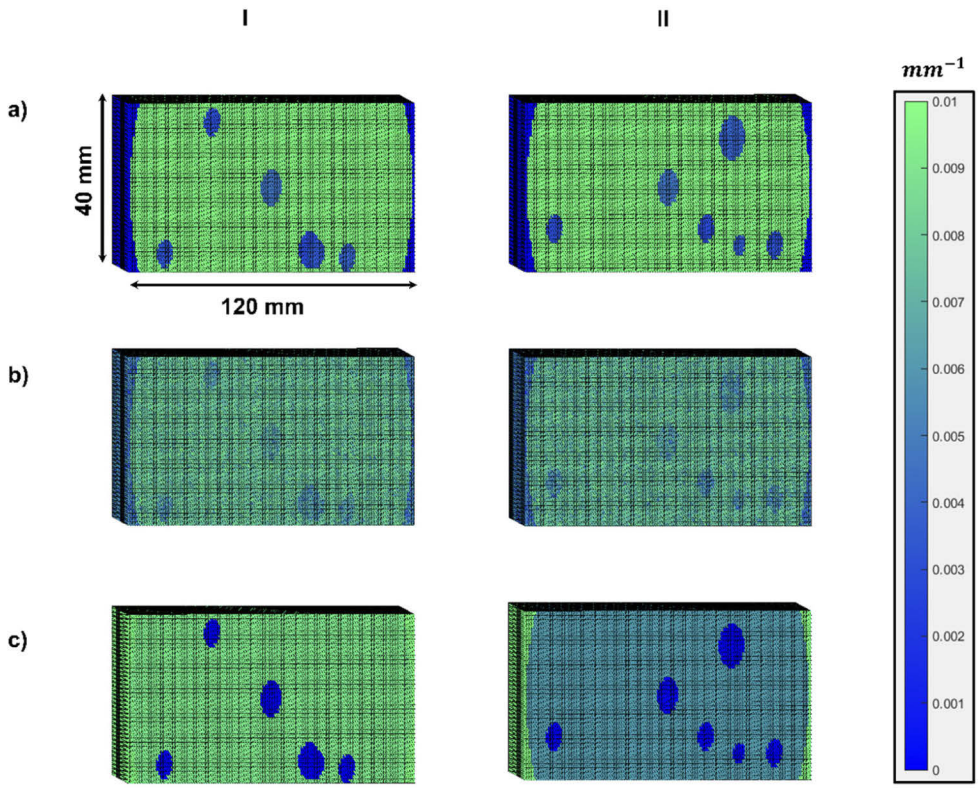

Fig. 7. I and II show the different breast tissues used to validate the neural network. The reconstructed absorption coefficients are shown. a) Shows the ground truths. b) Shows the image reconstruction by the analytical solution. c) Shows the image reconstruction by the neural network.

used to tackle inverse problems in DOT, and novel imaging and deep learning techniques can be developed to bring this optical imaging modality closer to real-time experimental procedures, as the findings of this study reveal.

4. Conclusions

This study investigated the potential use of feed-forward networks to solve inverse problems in DOT in compressed breast tissues. The results indicate that the cascaded feed-forward neural network algorithms are well-posed to solve inverse problems in DOT. Apart from being simple and consuming less time than other existing neural network methods, our proposed approach also delivers an excellent MSE of 0.0265 ± 0.0042 and a good R-value of 0.692 ± 0.023, showing the robustness and efficiency of the proposed neural network algorithm. As evident from Fig. 7, the reconstructed tumors' image contrast is also much better than other existing methods and analytical methods.

The proposed network's low MSE and high R values, and the accurate image reconstruction, show that the regression-based neural network approach provides a viable and efficient alternative to existing methods. It is the argument of the authors that this is due to solving the inverse problem using the neural network before reconstruction instead of using datasets for image reconstruction directly. Furthermore, multi-wavelength and structured light sources [46,47] can be employed to enhance the efficiency of the proposed deep-learning diffuse optical tomography

Biomedical Optics EXPRESS

model, and transfer learning can be applied to bridge the gap between simulations and imaging actual tissues paving the way for potential applications in biomedical optical engineering.

Funding. H2020 Future and Emerging Technologies (828978); Kreitman School of Advanced Graduate Studies, Ben-Gurion University of the Negev.

Acknowledgments. The authors thank the European Union's Horizon 2020 research and innovation programme (Future and Emerging Technologies) for funding the CancerScan Project. The authors also thank the Kreitman School of Advanced Graduate Studies and the Ben-Gurion University of the Negev for providing fellowships to continue the research.

Author Contributions: GMB and SA designed the study. GMB performed the numerical simulations. GMB and SA analyzed the data from numerical simulation. GMB constructed the feed-forward network and analyzed the result. Both the authors were involved in writing and reviewing the manuscript. GMB drew Figs. 1, 2, 3, and 4. The authors drew all the images or obtained the images through the study, and none of the images were taken from elsewhere. GMB drew Table 1.

Disclosures. The authors declare no conflict of interest.

Data availability. Data underlying the results presented in this paper is not publicly available at this time but may be obtained from the authors upon reasonable request.

References

1. Y. Zou, Y. Zeng, S. Li, and Q. Zhu, "Machine learning model with physical constraints for diffuse optical tomography," Biomed. Opt. Express **12**(9), 5720 (2021).
2. S. Yun, Y. Kim, H. Kim, S. Lee, U. Jeong, H. Lee, Y. Choi, and S. Cho, "Three-compartment-breast (3CB) prior-guided diffuse optical tomography based on dual-energy digital breast tomosynthesis (DBT)," Biomed. Opt. Express **12**(8), 4837 (2021).
3. L. Pereira, M. T. Ferreira, A. G. F. Lima, C. Salata, S. C. Ferreira-Machado, I. Lima, V. Morandi, and L. A. G. Magalhães, "Biological effects induced by doses of mammographic screening," Phys. Med. **87**, 90–98 (2021).
4. J. S. Drukteinis, B. P. Mooney, C. I. Flowers, and R. A. Gatenby, "Beyond mammography: new frontiers in breast cancer screening," Am. J. Med. **126**(6), 472–479 (2013).
5. N. Boldor, S. Vaknin, V. Myers, N. Hakak, M. Somekh, R. Wilf-Miron, and O. Luxenburg, "Reforming the MRI system: the Israeli National Program to shorten waiting times and increase efficiency," Isr. J. Health Policy Res. **10**(1), 57 (2021).
6. P. Taroni, "Diffuse optical imaging and spectroscopy of the breast: a brief outline of history and perspectives," Photochem. Photobiol. Sci. **11**(2), 241–250 (2012).
7. M. H. Nguyen, Y. Zhang, F. Wang, J. De La Garza Evia Linan, M. K. Markey, and J. W. Tunnell, "Machine learning to extract physiological parameters from multispectral diffuse reflectance spectroscopy," J. Biomed. Opt. **26**(5), 052912 (2021).
8. I. Fredriksson, M. Larsson, and T. Strömberg, "Machine learning for direct oxygen saturation and hemoglobin concentration assessment using diffuse reflectance spectroscopy," J. Biomed. Opt. **25**(11), 112905 (2020).
9. T. Vo-Dinh, *Biomedical Photonics: Handbook* (Routledge, 2003).
10. L. V. Wang and H.-I. Wu, *Biomedical Optics: Principles and Imaging* (Wiley, 2012).
11. S. Sabir, S. Cho, Y. Kim, R. Pua, D. Heo, K. H. Kim, Y. Choi, and S. Cho, "Convolutional neural network-based approach to estimate bulk optical properties in diffuse optical tomography," Appl. Opt. **59**(5), 1461 (2020).
12. S. L. Jacques, "Optical properties of biological tissues: a review," Phys. Med. Biol. **58**(11), R37–R61 (2013).
13. A. A. Leino, A. Pulkkinen, and T. Tarvainen, "ValoMC: a Monte Carlo software and MATLAB toolbox for simulating light transport in biological tissue," OSA Continuum **2**(3), 957 (2019).
14. H. Dehghani, M. E. Eames, P. K. Yalavarthy, S. C. Davis, S. Srinivasan, C. M. Carpenter, B. W. Pogue, and K. D. Paulsen, "Near infrared optical tomography using NIRFAST: Algorithm for numerical model and image reconstruction," Commun. Numer. Methods Eng. **25**(6), 711–732 (2009).
15. M. Schweiger and S. Arridge, "The Toast++ software suite for forward and inverse modeling in optical tomography," J. Biomed. Opt. **19**(4), 040801 (2014).
16. Y. Zhao, Y. Deng, S. Yue, M. Wang, B. Song, and Y. Fan, "Direct mapping from diffuse reflectance to chromophore concentrations in multi-fx spatial frequency domain imaging (SFDI) with a deep residual network (DRN)," Biomed. Opt. Express **12**(1), 433 (2021).
17. H. Wang, F. Xia, G. Han, Z. Zhao, H. Chen, and J. Wang, "Optical parameters detection with multi-frequency modulation based on NIR DPDW," Infrared Phys. Technol. **97**, 135–141 (2019).
18. R. A. Stillwell, V. J. Kitsmiller, and T. D. O'Sullivan, "Towards a high-speed handheld frequency-domain diffuse optical spectroscopy deep tissue imaging system," in *Optics InfoBase Conference Papers* (2020), Part F178.
19. L. Zhang, B. Cao, X. He, Z. Sun, J. Li, Z. Zhou, and F. Gao, "High-sensitive multiwavelength dynamic diffuse optical tomography system: a preliminary investigation," Front. Phys. **8**, 600812 (2020).
20. J. Yoo, S. Sabir, D. Heo, K. H. Kim, A. Wahab, Y. Choi, S. I. Lee, E. Y. Chae, H. H. Kim, Y. M. Bae, Y. W. Choi, S. Cho, and J. C. Ye, "Deep Learning Diffuse Optical Tomography," IEEE Trans. Med. Imaging **39**(4), 877–887 (2020).

Biomedical Optics EXPRESS

21. H. Ben Yedder, A. BenTaieb, M. Shokoufi, A. Zahiremami, F. Golnaraghi, and G. Hamarneh, "Deep learning based image reconstruction for diffuse optical tomography," in *Lecture Notes in Computer Science* (Including Subseries Lecture Notes in Artificial Intelligence and Lecture Notes in Bioinformatics) (2018), 11074 LNCS, pp. 112–119.
22. H. Ben Yedder, B. Cardoen, and G. Hamarneh, "Deep learning for biomedical image reconstruction: a survey," Artif. Intell. Rev. **54**(1), 215–251 (2021).
23. H. Ben Yedder, M. Shokoufi, B. Cardoen, F. Golnaraghi, and G. Hamarneh, "Limited-angle diffuse optical tomography image reconstruction using deep learning," in *Lecture Notes in Computer Science* (Including Subseries Lecture Notes in Artificial Intelligence and Lecture Notes in Bioinformatics) (2019), 11764 LNCS, pp. 66–74.
24. H. Gupta, K. H. Jin, H. Q. Nguyen, M. T. McCann, and M. Unser, "CNN-based projected gradient descent for consistent CT Image Reconstruction," IEEE Trans. Med. Imaging **37**(6), 1440–1453 (2018).
25. D. Liang, J. Cheng, Z. Ke, and L. Ying, "Deep MRI reconstruction: unrolled optimization algorithms meet neural networks," arXiv (2019).
26. A. Dhillon and G. K. Verma, "Convolutional neural network: a review of models, methodologies and applications to object detection," Prog. Artif. Intell. **9**(2), 85–112 (2020).
27. B. Deng, H. Gu, and S. A. Carp, "Deep learning enabled high-speed image reconstruction for breast diffuse optical tomography," in (2021), p. 7.
28. M. B. Applegate, R. E. Istfan, S. Spink, A. Tank, and D. Roblyer, "Recent advances in high speed diffuse optical imaging in biomedicine," APL Photonics **5**(4), 040802 (2020).
29. G. M. Balasubramaniam, B. Wiesel, N. Biton, R. Kumar, J. Kupferman, and S. Arnon, "Tutorial on the use of deep learning in diffuse optical tomography," Electronics **11**(3), 305 (2022).
30. G. M. Balasubramaniam and S. Arnon, "Deep-learning algorithm to detect anomalies in compressed breast: a numerical study," in *Biophotonics Congress*, OSA Technical Digest (Optical Society of America, 2021), p. paper DTu3A.5.
31. P. Nanglia, A. N. Mahajan, D. S. Rathee, and S. Kumar, "Lung cancer classification using feed forward back propagation neural network for CT images," Int. J. Med. Eng. Inform. **12**(5), 447–456 (2020).
32. D. H. Ye, G. T. Buzzard, M. Ruby, and C. A. Bouman, "Deep back projection for sparse-view CT reconstruction," in *2018 IEEE Global Conference on Signal and Information Processing*, GlobalSIP 2018 - Proceedings (2019), pp. 1–5.
33. S. Lohit, K. Kulkarni, R. Kerviche, P. Turaga, and A. Ashok, "Convolutional neural networks for noniterative reconstruction of compressively sensed images," IEEE Trans. Comput. Imaging **4**(3), 326–340 (2018).
34. J.-M. Kaltenbach, "Frequency- and time-domain modelling of light transport in random media," Proc. SPIE **10311**, 1031106 (1993).
35. Q. Fang and D. A. Boas, "Monte Carlo simulation of photon migration in 3D turbid media accelerated by graphics processing units," Opt. Express **17**(22), 20178 (2009).
36. M. Bertero and P. Boccacci, *Introduction to Inverse Problems in Imaging* (Routledge, 2020).
37. K. M. S. Uddin, A. Mostafa, M. Anastasio, and Q. Zhu, "Two step imaging reconstruction using truncated pseudoinverse as a preliminary estimate in ultrasound guided diffuse optical tomography," Biomed. Opt. Express **8**(12), 5437 (2017).
38. W. F. Cheong, S. A. Prahl, and A. J. Welch, "A review of the optical properties of biological tissues," IEEE J. Quantum Electron. **26**(12), 2166–2185 (1990).
39. M. Pinto, R. Egging, A. Rodríguez-Ruiz, K. Michielsen, and I. Sechopoulos, "Compressed breast shape characterization and modelling during digital breast tomosynthesis using 3D stereoscopic surface cameras," Proc. SPIE **11513**, 1151307 (2020).
40. B. W. Pogue, T. O. McBride, U. L. Osterberg, and K. D. Paulsen, "Comparison of imaging geometries for diffuse optical tomography of tissue," Opt. Express **4**(8), 270 (1999).
41. D. Grosenick, H. Wabnitz, K. T. Moesta, J. Mucke, P. M. Schlag, and H. Rinneberg, "Time-domain scanning optical mammography: II. Optical properties and tissue parameters of 87 carcinomas," Phys. Med. Biol. **50**(11), 2451–2468 (2005).
42. S. A. Prahl, "A Monte Carlo model of light propagation in tissue," Proc. SPIE **10305**, 1030509 (1989).
43. M. Matsumoto and T. Nishimura, "Mersenne twister: a 623-dimensionally equidistributed uniform pseudo-random number generator," in *ACM Transactions on Modeling and Computer Simulation* (1998), 8(1), pp. 3–30.
44. A. Hauptmann and B. Cox, "Deep learning in photoacoustic tomography: current approaches and future directions," J. Biomed. Opt. **25**(11), 112903 (2020).
45. T. Feng, P. Edström, and M. Gulliksson, "Levenberg-Marquardt methods for parameter estimation problems in the radiative transfer equation," Inverse Probl. **23**(3), 879–891 (2007).
46. G. M. Balasubramaniam, N. Biton, and S. Arnon, "Imaging through diffuse media using multi-mode vortex beams and deep learning," Sci. Rep. **12**(1), 1561 (2022).
47. N. Biton, J. Kupferman, and S. Arnon, "OAM light propagation through tissue," Sci. Rep. **11**(1), 2407 (2021).